The role of oxygen defects on the Electronic, Optical and Phonon Dispersion of LAGO Perovskite: A Density Functional Investigation

Chaithanya P. Bhat, Ashwin K. Godbole and Debashis Bandyopadhyay*
Department of Physics, Birla Institute of Technology and Science Pilani
Pilani, Rajasthan – 333031, INDIA
*e-mail: Debashis.bandy@gmail.com

Supplementary Information

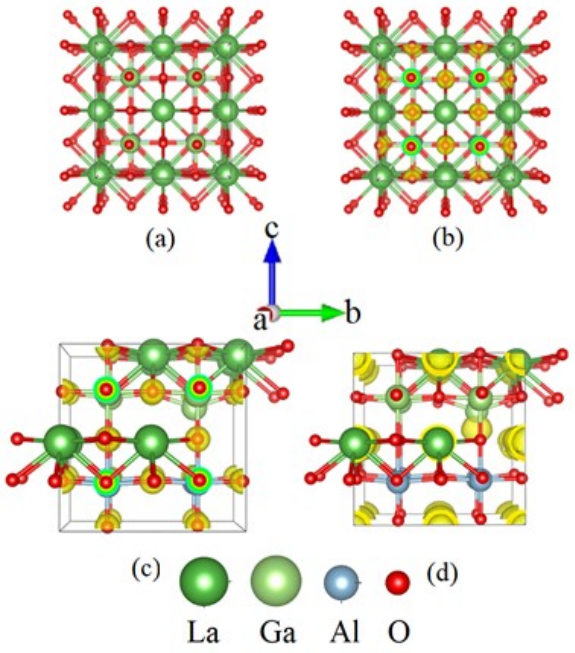

SI Fig. 1. (a) Structure of $La_8Al_4Ga_4O_{24}$ supercell, (b) Charge density distribution on the supercell, (c) Charge density difference between pure and Oxygen vacancy induced supercell, (d) The yellow spheres is the ELF charge at the vacancy sites of the supercell.

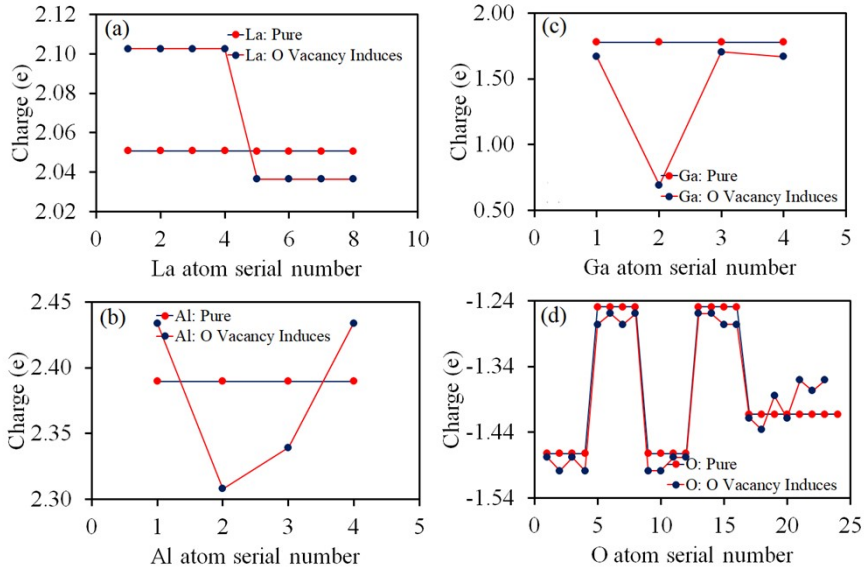

SI Fig. 2. Bader charges on different atoms. (a) La, (b) Al, (c) Ga, and (d) O.

SI Table 1: Bader charge on different elements of $La_8Al_4Ga_4O_{24}$ supercell

Elements	Number	Bader charge	Bader charge	Elements	Number	Bader charge	Bader charge
		Pure	O Vacancy			Pure	O Vacancy
La1	1	2.051	2.102	**O5**	5	-1.25	-1.276
La2	2	2.051	2.102	**O6**	6	-1.25	-1.260
La3	3	2.051	2.102	**O7**	7	-1.25	-1.276
La4	4	2.051	2.102	**O8**	8	-1.25	-1.259
La5	5	2.051	2.037	**O9**	9	-1.473	-1.499
La6	6	2.051	2.037	**O10**	10	-1.473	-1.499
La7	7	2.051	2.037	**O11**	11	-1.473	-1.478
La8	8	2.051	2.037	**O12**	12	-1.473	-1.478
Al1	1	2.39	2.434	**O13**	13	-1.25	-1.260
Al2	2	2.39	2.308	**O14**	14	-1.25	-1.260
Al3	3	2.39	2.339	**O15**	15	-1.25	-1.276
Al4	4	2.39	2.434	**O16**	16	-1.25	-1.276
Ga1	1	1.778	1.669	**O17**	17	-1.413	-1.418
Ga2	2	1.778	0.694	**O18**	18	-1.413	-1.436
Ga3	3	1.778	1.704	**O19**	19	-1.413	-1.385
Ga4	4	1.778	1.669	**O20**	20	-1.413	-1.418
O1	1	-1.473	-1.478	**O21**	21	-1.413	-1.361
O2	2	-1.473	-1.498	**O22**	22	-1.413	-1.377
O3	3	-1.473	-1.478	**O23**	23	-1.413	-1.361
O4	4	-1.473	-1.498	**O24**	24	-1.413	

Phonon Dynamics

It is known that the phonons are quantized modes of lattice vibrations in transverse and longitudinal modes. When two or more charged particles in a primitive cell move in opposite directions with the center of mass at rest, the result is optical phonons. This model has the highest energy at the gamma point of the lattice. Acoustic phonons are associated with the propagation of the longitudinal lattice vibration mode. They are low-energy vibrations due to the collective motion of the crystal lattice's relatively heavier atoms (metallic). The energy of the acoustic phonons is minimal at the gamma point. Therefore, the curvature of the acoustic phonons and the optical phonons at the gamma point are opposite. The frequency of the acoustic phonons is directly proportional to their wave vector of oscillations. In three-dimensional solids, the two optical branches and one acoustic phonon bunch are related to the transverse and longitudinal modes. The optical phonon frequencies fall in the IR or visible light region. The leading cause of the generation of these high-frequency optical phonons is due to the stretching or bending mode in lattice oscillations. Usually, the optical phonons have a non-linear dispersion relation, which means the frequency is not directly proportional to the wave vector of the oscillation modes. In three-dimensional solids, there can be multiple branches of optical phonons. The distinction between acoustic and optical phonons is primarily based on their energy and the type of lattice vibrations involved. Since thermal conductivity is due to the vibration of atoms in the solids, the acoustic phonons contribute considerably to the thermal properties, such as thermal conductivity and heat capacity of the materials.

On the other hand, optical phonons play a crucial role in various optical phenomena of the materials, i.e., absorption and scattering of light and interactions with the bound electrons in materials. Therefore, studying acoustic and optical phonon bands may give valuable information about the materials' thermal, mechanical, and electronic properties.

The present study's calculated phonon bands (**Fig. 4)** are discontinuous at most Brillion zone boundaries. The lattice vibration affects the phonon dispersion and the thermal conductivity at different directions of the crystal lattice, especially at the Brillion zone boundaries. The thermal conductivity can be higher along specific crystallographic directions with steeper phonon dispersion curves between Brillion zone boundaries (mainly, about Γ point) and lower along the other direction where the curves have lower slopes. It is to be noted that the phonon bands (in the acoustic region) at the Gamma point in the crystal lattice are symmetrical, and the slope is steeper towards the k-path boundaries. Hence, in the region of the 1st Brillouin zone, the thermal conductivity would be maximum and uniform in all directions. Compared to the pure LAGO, the slopes in the exact Brillion zone boundaries in Oxygen vacancy-

induced LAGO are less. Still, at the same time, this is more widely distributed in the other direction in the K-path. However, the slope varies in different Brillion zone boundaries along the K-path. Concerning **Fig. 4**, careful observation shows that the bands are continuous in the low-frequency region, and within the Brillion zone Γ→M→X→Γ→R→X and R→M, the bands are continuous.

Hence, the dispersion is less. A nondegenerate mode has been found at the X point. It stiffens up rapidly away from the X point. It indicates that neighboring chains of oxygen atoms displace in opposite directions. The acoustic phonon spectrum extends to the phonon frequency close to 10 THz in both systems. At the boundary, the bands degenerate and follow a different curvature. The branches are distributed uniformly up to 20 THz along all three directions. However, the phonon band densities differ in pure and vacancy-induced LAGOs. In vacancy-induced LAGO, the optical regions moved downward with a small value of phonon band gap, which is very clear from the corresponding PDOS plots. In the PDOS, the acoustic phonon contributions are mainly from the La, Al, and Ga. The optical PDOS and, hence, the optical phonon bands are due to the oxygen atoms. In the phonon dispersion and PDOS spectrum, the optical modes are divided into two distinct groups, corresponding to the low-frequency and high-frequency modes. The peak corresponding to the high-frequency modes is broader and has a higher intensity than those corresponding to the low-frequency modes. In the vacancies-induced LAGO, the optical phonon bands and PDOS distribution are less wide than the pure LAGO. A clear band appears above 20 THz in the vacancy-induced LAGO, possibly due to the color centers created due to the vacancies.

Thermodynamic Properties

We calculated the Debye temperature from the following equation, where the Debye temperature has a significant role in the variation of C_v with temperature [**1**]. A detailed discussion of the thermodynamic properties is given in the supplementary materials.

$$C_V = 9Nk_B\left(\frac{T}{\Theta_D}\right)^3 \int_0^{x_D} \frac{x^4.e^x.dx}{\left(e^x-1\right)^2}\ ;where,\ x_D = \frac{T}{\Theta_D}; x = \frac{\hbar\omega}{k_BT}; k_B = Boltzmann\ constant, \Theta_D = Debye\ Temperature$$

The calculated Debye temperatures for these two systems are 469.92 K and 463.69 K, respectively. The higher the melting point of a substance, the more substantial the atomic bonding force and the higher the Debye temperature. Due to inducing defects, the system bond strengths become weaker and are expected to reduce the melting point. From the calculated values of Debye temperature, the lower value in the induced system supports this. It is known that the

degrees of freedom in lattice vibrations play an essential role in the thermodynamic parameters compared to the electronic degrees of freedom. The temperature dependence of the Helmholtz free energy (F), entropy (S), and constant-volume heat capacity (Cv) are calculated within the limit of harmonic approximation following the expression reported earlier.

$$F(T) = E_{Total} + \frac{1}{2}\int g(\omega)\hbar\omega.d\omega + k_B T\int g(\omega)ln\left(1 - e^{\frac{\hbar\omega}{k_B T}}\right)$$

$$S(T) = k_B\left[\int \frac{\frac{\hbar\omega}{k_B T}}{e^{\frac{\hbar\omega}{k_B T}} - 1} g(\omega).d\omega - \int g(\omega)ln\left(1 - e^{\frac{\hbar\omega}{k_B T}}\right).d\omega\right],$$

As shown in Fig. 5, in pure and vacancy-induced systems, the Gibbs free energy decreases with the increase in temperature. The Free energy is zero at 321K and 331K in pure and vacancy systems, respectively. Zero Gibb's Free energy indicates the equilibrium temperature of the system. A small change in the equilibrium temperature between the pure and vacancy-induced systems also supports the structural change in the system due to vacancies. On the other hand, the entropy and heat capacity increase from zero per the third law of thermodynamics. The rate of change of these two parameters is slightly higher in a pure system. It is to be noted that below the Debye temperature, the nature of the variation of C_v is different in the two systems. The tendency to reach saturation value is faster in vacancy-induced systems than in pure systems. At lower temperatures (much lower than the Debye temperatures), the heat capacity C_v is proportional to T^3. The contribution in lattice heat capacity at low temperatures is from the lattice's low frequency or long wavelength acoustic phonon vibration modes. However, C_v tends to the Dulong–Petit classical limit at high temperatures.

References:

1. S. Baroni, S. de Gironcoli, A. Dal Corso and P. Giannozzi, Rev. Mod. Phys., 2001, 73, 515–562, https://doi.org/10.1103/RevModPhys.73.515